ELSEVIER

Ceramics International 25 (1999) 649–659

CERAMICS INTERNATIONAL

Microstructure of a sialon composite prepared by hot pressing and reactive sintering of β-Si_3N_4 coated with amorphous Al_2O_3

G. Ghosh*, S. Vaynman, M.E. Fine

Department of Materials Science and Engineering, Robert R. McCormick School of Engineering and Applied Science, Northwestern University, 2225 N. Campus Drive, Evanston, IL 0208-3108, USA

Received 26 November 1997; received in revised form 14 June 1998; accepted 3 August 1998

Abstract

A composite microstructure, consisting of β-sialon, O-sialon and X-sialon phases, was produced by coating β-Si_3N_4 particles with amorphous alumina followed by hot pressing and reactive sintering at 1923 K. The microstructure, chemistry of the phases and interphase interfaces of this ceramic were characterized by TEM and high resolution AEM. Both polyhedral and elongated β-sialon grains were observed. TEM examination showed the formation of a large number of β-sialon grains and PEELS and EDS X-ray microanalysts in AEM revealed they had varying amounts of aluminum and oxygen contents. HREM examination of several interphase interfaces and triple junctions suggests that the amount of glassy phase in the produced ceramic is substantially lower compared to those reported in the literature. This is of importance for high temperature properties.

Keywords: B. Microstructure; D. Sialon composite

1. Introduction

Silicon nitride-based or sialon ceramics are increasingly being considered for many engineering applications due to their low density, high strength, and high elastic modulus. For many engineering applications, sialon ceramics are required to have, among many other properties, both high fracture toughness and good tribological properties. Recently, nearly fully dense sialon ceramics having fracture toughness 6 to 10 MPa$\sqrt{m}$ have been produced [1–6]. In order to circumvent extremely sluggish diffusivity of nitrogen in α- and β-Si_3N_4, dense sialon ceramics are produced by liquid-phase sintering of α-Si_3N_4. This is achieved by adding, in general, a combination of various sintering aids, such as AlN, Al_2O_3, HfO_2, BeO, Be_3N_2, MgO, Mg_2N_3, Re_2O_3 (Re = Ce, Dy, Gd, La, Sm, Tb, Y, Yb), SiO_2, ZrC, ZrN and ZrO_2. Depending on the additives, temperatures in the range of 1350 to 1950°C have been used by different research groups for liquid-phase sintering that yields polyphase materials having crystalline grains bonded by an intergranular phase. Typically, an interlocking microstructure consisting of β-Si_3N_4 and/or β-sialon grains is produced with a residual glassy or partly crystalline grain boundary phase. The fracture process in such a microstructure is predominantly intergranular, where the cracks tend to follow a tortuous path. However, the presence of an intergranular glassy phase causes rapid deterioration of properties at temperatures above the glass transition temperature [7]. Therefore, to improve high-temperature properties of these ceramics, it is desirable to minimize, and, if possible, to eliminate the intergranular glassy phase.

With respect to Si_3N_4 two approaches can lead to significant improvement in the high-temperature properties. The first is the use of high-purity Si_3N_4 starting powder and minimizing the amount of additives required. That has resulted in some improvement of properties; however, the high-temperature properties are still inherently limited by the properties of the glassy phase. The second approach is to eliminate the glassy phase through a crystallization process, with the resultant formation of a refractory hard material as a secondary grain boundary phase [8,9]. A theoretical model based on thermodynamics and kinetics has shown that crystallization of small quantities of glass at grain boundaries is more difficult than crystallization of a bulk glass [10]. Experimentally, complete crystallization

* Corresponding author.

0272-8842/99/$ - see front matter
PII: S0272-8842(98)00079-0

of intergranular glassy films has never been achieved [8,11].

Conventional powder blending involves milling/mixing processes in which the raw materials are ground with the sintering additive(s) in a milling device. One of the primary objectives of synthesis of structural ceramics is to minimize the proportion of sintering aid and to improve homogeneity, reproducibility and sinter activity. In conventional powder blending processes the homogeneity of the additive distribution is limited by the particle size distribution of the starting powders. Furthermore, this method is not well suited for the doping of Si_3N_4 with small amounts of sintering additive. Particle coating techniques are receiving increasing attention as they offer several advantages. They provide a convenient means of incorporating sintering aids and dopants more uniformly than can be obtained by conventional powder blending [12–16]. Uniform powder coating results in maximizing the initial area of contact, more surface diffusion and hence accelerated kinetics, increase in surface nucleation sites (relevant to the formation of sialon) and better microstructural homogeneity. Such microstructural uniformity is highly desirable for improving the mechanical properties and Weibull modulus. The objectives of the present work were to consolidate β-Si_3N_4 powders coated with alumina and to investigate the microstructural evolution after hot pressing and reactive sintering. To promote copious heterogeneous nucleation of β-sialon grains, β-Si_3N_4 powder was selected as a starting material.

2. Experimental procedure

Silicon nitride powder (95% β-Si_3N_4) was received from SIGMA Corporation (USA). Particle size was found to lie between 0.3 and 1.0 μm. An aluminum hydroxide coating was applied on the β-Si_3N_4 particles using the technique described by Nakamura and Kato [17]. Aluminum sulfate hydrate and urea (ACS reagent grades) needed for this purpose were obtained from Aldrich Chemical Company, USA.

The β-Si_3N_4 particles were suspended and agitated in a solution of aluminum sulfate pre-heated to 353 K. Urea was added to precipitate aluminum hydroxide according to following reaction:

$$Al_2(SO_4)_3 + 3CO(NH_2)_2 + 9H_2O \rightarrow 2Al(OH)_3 + 3(NH_4)_2SO_4 + 3CO_2 \quad (1)$$

At the beginning of the deposition process the pH was between 1.5 and 2.5 (depending on the amount of ingredients). During deposition the pH gradually rose and, when the deposition was complete, i.e. practically all aluminum sulfate was consumed, the pH rapidly rose to ~5. After deposition of aluminum hydroxide, the Si_3N_4 particles were cleaned with methanol and centrifuged out of the suspension. They were dried at 423 K for 20 h and then calcined at 1173 K for 30 min. Hot-pressing of alumina-coated silicon nitride powder, without using any binder, was carried out in a graphite mould at 1923 K for 1 h and at a pressure of 51.71 MPa in nitrogen atmosphere. The pressed pellets were sintered at 1923 K in a tube furnace in a nitrogen atmosphere for 72 h.

The microstructure of as-coated and hot-pressed and reactive sintered samples were characterized by various electron microscopy techniques. Conventional transmission electron microscopy was carried out in a Hitachi 700H transmission electron microscope (TEM). High-resolution electron microscopy (HREM) and analytical characterization were performed in a cold field emission gun high resolution analytical electron microscope (AEM, Hitachi HF-2000), which is equipped with a Gatan 666 parallel electron energy loss spectrometry (PEELS) detector, an ultrathin window (ATW) Link energy dispersive X-ray (EDS) detector and data processor (QX2000) and a Gatan CCD camera for HREM imaging. Both microscopes were operated at 200 kV. An LN_2 specimen holder was used, except for the interphase studies, to collect PEELS and EDS X-ray spectra. Alumina-coated Si_3N_4 particles were collected on a holey carbon film for TEM/AEM characterization. Discs of 3 mm diameter were cut from the hot-pressed and sintered sample, and subjected to dimpling and ion-milling to electron transparency in a Gatan 600 Dual Ion Mill. X-ray diffraction of hot-pressed and sintered sample was carried out on a polished surface in a Scintag XDS2000 diffractometer using CuK_α radiation.

3. Results and discussion

3.1. Density of the produced ceramic

Chemical analysis of the powders after coating and calcination gave 49.4 wt% Si, 31.2 wt% N, 10.5 wt% O, 8.8 wt% Al, and 200 ppm of CaO. Assuming that all excess oxygen and silicon are in the form of SiO_2, this will correspond to 78.31 wt% Si_3N_4, 5.02 wt% SiO_2, and 16.65 wt% Al_2O_3. The discs produced after hot pressing and reactive sintering had a density of 2970 kg/m^3. As will be shown later, the produced ceramic consists of three phases: β-sialon ($Si_{6-z}Al_zO_zN_{8-z}$), O-sialon and X-sialon. Theoretical densities of these phases are $3200-41z$ [18], 2820 [19], and 3010 kg/m^3 [20], respectively. Based on the subsolidus phase diagram given by Naik et al. [21], the phase fractions were estimated to be 0.72 of β-sialon with $z=0.74$, 0.21 of O-sialon and 0.07 of X-sialon. This corresponds to a theoretical density of 3085 kg/m^3. Thus, the measured density is approximately 96.5% of theoretical density.

3.2. TEM examination of as-coated powders

Fig. 1 shows a bright-field (BF) TEM micrograph of an alumina coated Si_3N_4 particle. Most of the observed Si_3N_4 particles were approximately 400 nm in size and irregular in shape. While the particle in Fig. 1 is coated somewhat uniformly, coatings of highly non-uniform thickness were also observed. The alumina-coating thickness for most of the particles was in the range of 10 to 50 nm. Selected area diffraction patterns (SADP) from the coating suggest that it is predominantly amorphous in nature; however, occasionally sharp spots were also noticed along with diffuse rings indicating the nanocrystalline nature of the coating.

The experimental variables that govern the as-coated microstructure are: (i) the solution temperature, (ii) reactant concentration, (iii) pH of the solution. These parameters have significant influence on the microstructural parameters, such as the thickness of the coating, particle agglomeration and the structure of the coating (amorphous vs nanocrystalline). At lower pH the Si_3N_4 particles tend to disperse uniformly in the solution, whereas agglomeration is likely to occur at higher pH levels. The pH level also controls the crystallinity of the coating; at pH less than ~7, amorphous aluminum hydroxide coatings are produced, whereas crystalline (pseudo-boehmite or bayerite) coatings are produced at pH greater than ~8. To promote uniform spatial distribution of β-sialon in the sintered microstructure, an amorphous aluminum hydroxide coating is preferred. Wang and Riley [14] have investigated the stability of a nanocrystalline alumina coating on α-Si_3N_4. They found that, due to very high specific surface area, the nanoparticles are inherently unstable with respect to grain growth and they undergo coarsening during heating to the sintering temperature, which ultimately leads to non-uniform distribution of the alumina particles. Even so, they concluded that the powder coating technique offers significant advantages over the conventional powder-blending method.

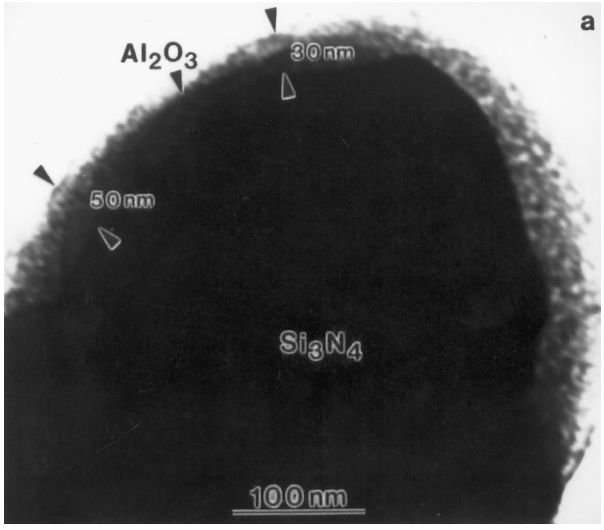

Fig. 1. Bright-field TEM micrograph of as-coated β-Si_3N_4 particle showing uniform alumina coating.

3.3. Microstructure after hot-pressing and sintering

Fig. 2(a)–(d) shows bright-field TEM micrographs of hot-pressed and reactive sintered sample. The presence of both polyhedral (irregular in shape) and elongated grains may be noticed. In general β-sialon grains were found to have a wide variety of aspect ratios. TEM structural analysis showed that β-sialon grains grow preferentially along the [0001] direction, thus confirming a previous report [22]. Polyhedral grains of β-sialon that do not appear to be hexagonal prisms were also observed. At least 15 EDS X-ray spectra were collected from different β-sialon grains showing varying amounts of aluminum and oxygen contents, suggesting that the β-sialon grains may have nucleated and grown under a variety of conditions.

Traditionally, the development of an interlocking network of β-sialon grains has been interpreted by a solution/precipitation mechanism, which is brought about by forming a low-melting liquid at the sintering temperature. In the conventional sintering procedure starting with predominantly α-Si_3N_4, various sintering aids are intentionally added to form a low-melting liquid that is also highly saturated with nitrogen. Formation of this nitrogen-saturated oxide melt is thought to trigger the precipitation of β-sialon [22,23]. Energetically, β-Si_3N_4 should be preferred nucleation sites for β-sialon due to the similar stacking sequence and small difference in lattice parameter, thus smaller interfacial energy and strain energy, respectively. In such a case epitaxial nucleation may be favored [22]. The parallel arrangement of the β-sialon grain shown in Fig. 2(d) is suggestive of epitaxial nucleation on β-Si_3N_4 grain. It is unlikely that the parallel arrangement is an effect of applied stress as both parallel and non-parallel arrangements were noticed in the microstructure. Observation of very large β-sialon grains, though occasionally, surrounding β-Si_3N_4 may imply either nucleation and growth from a liquid phase or an abnormal grain growth as has been demonstrated by Emoto and Mitomo [24]. The β-sialon grains shown in Fig. 3(a) and (b) are much larger than those shown in Fig. 2.

Sintering of predominantly β-Si_3N_4 has demonstrated [25–27] that transformation from α- to β-Si_3N_4 during sintering is not necessary for densification, rather it has a significant influence on grain growth. Furthermore, it has been concluded that predominantly β-Si_3N_4 powder can be used to produce denser materials compared to α-Si_3N_4, although the latter is preferred to obtain a combination of fine and elongated grains for higher fracture toughness [26]. The evolution of sintered microstructure

depends strongly on the α/β ratio in the starting powder. The starting powder used contained ~95 volume percent of β-Si_3N_4. The size distribution of the β-particles also plays an important role in the development of the final microstructure. If the starting powder contains large and small β-Si_3N_4 particles, the smaller particles start to dissolve into the liquid phase due to their higher chemical potential. The dissolved species tend to precipitate on

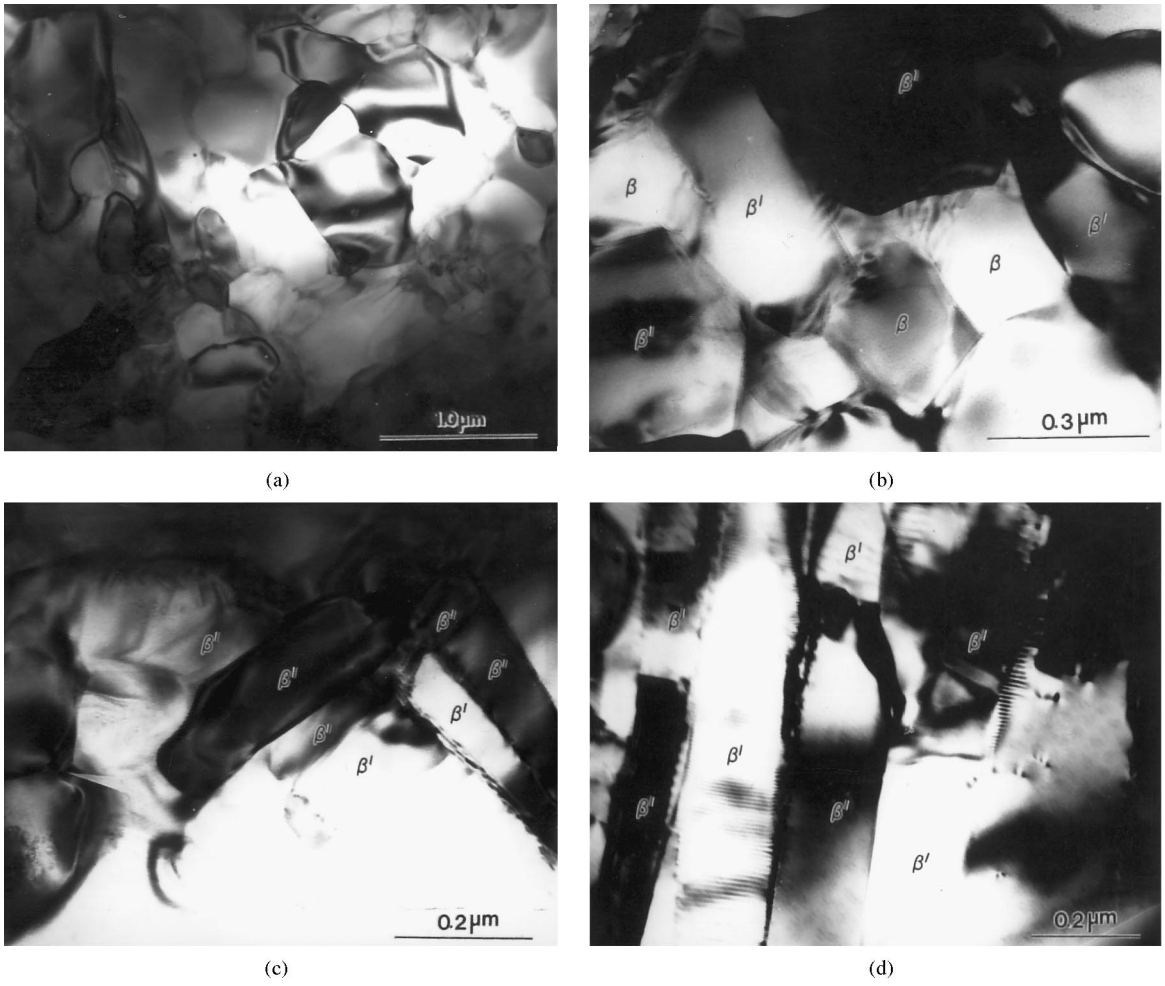

Fig. 2. Bright-field TEM micrographs of coated, hot pressed and reactive sintered silicon nitride: (a) at low magnification, (b) both elongated and polyhedral β-sialon, (c) β-sialon grains with variable aspect ratios, and (d) parallel arrangement of β-sialon grains.

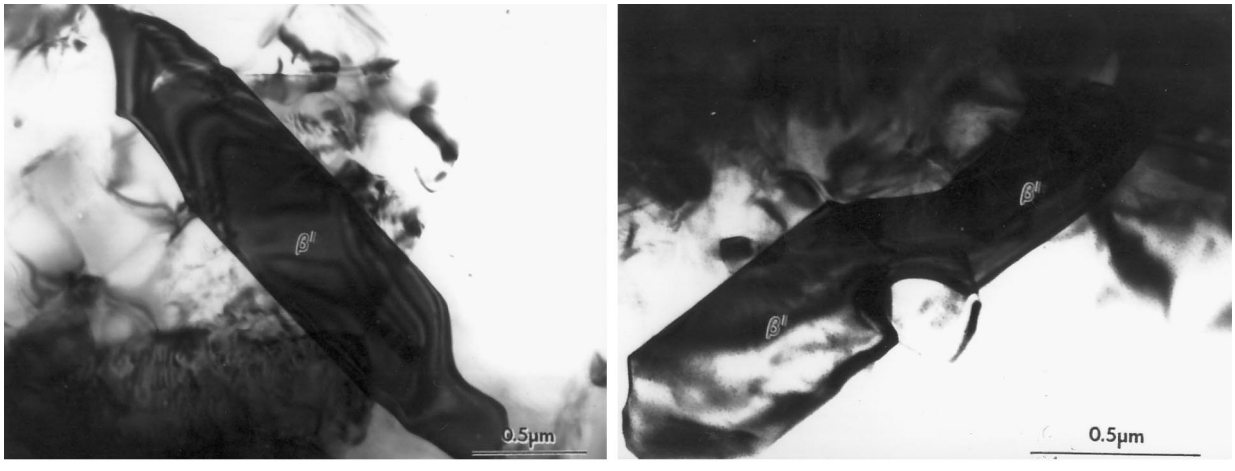

Fig. 3. Large β-sialon grains (a and b) surrounded by β-Si_3N_4 grains.

the larger existing β-Si_3N_4 which leads to the reduction of surface energy. This process leads to spherical or equiaxed grains initially, but their final growth morphology may be different due to a faceting transition. Even in a powder mixture containing 95 volume percent of β-Si_3N_4, some regions will be locally very rich in α-Si_3N_4 and cause high supersaturation with respect to β-Si_3N_4. This may result in spontaneous nucleation of β-sialon, which may grow into idiomorphic rod-like grains, in a manner similar to the microstructural evolution during sintering of high-volume percent α-Si_3N_4. This appears to be consistent with the occasional observation of very large β-sialon grains shown in Fig. 3(a) and (b). Results shown in Figs. 2 and 3 demonstrate that a large number of β-sialon grains having varying shape, size and chemistry have formed during sintering. Unreacted and β-Si_3N_4 grains, probably be due to particle agglomeration, in contact with β-sialon were also observed [see Fig. 2(b)].

Fig. 4(a) shows a bright-field TEM micrograph of O-sialon grains characterized by their elongated shape and the presence of a high density of defects arranged in a parallel manner. O-sialon has an orthorhombic structure [28] and has high density of stacking faults parallel to the (100) planes. As has been reported previously [29], contrast variation within the grains caused by the strain fields of the defects may be noted in Fig. 4(a). Fig. 4(b) and (c) show two SADPs from the O-sialon grains, and they are indexed in terms of the orthorhombic structure. Fig. 4(d) is an EDS X-ray spectrum from the O-sialon showing high oxygen intensity relative to nitrogen and very little aluminum.

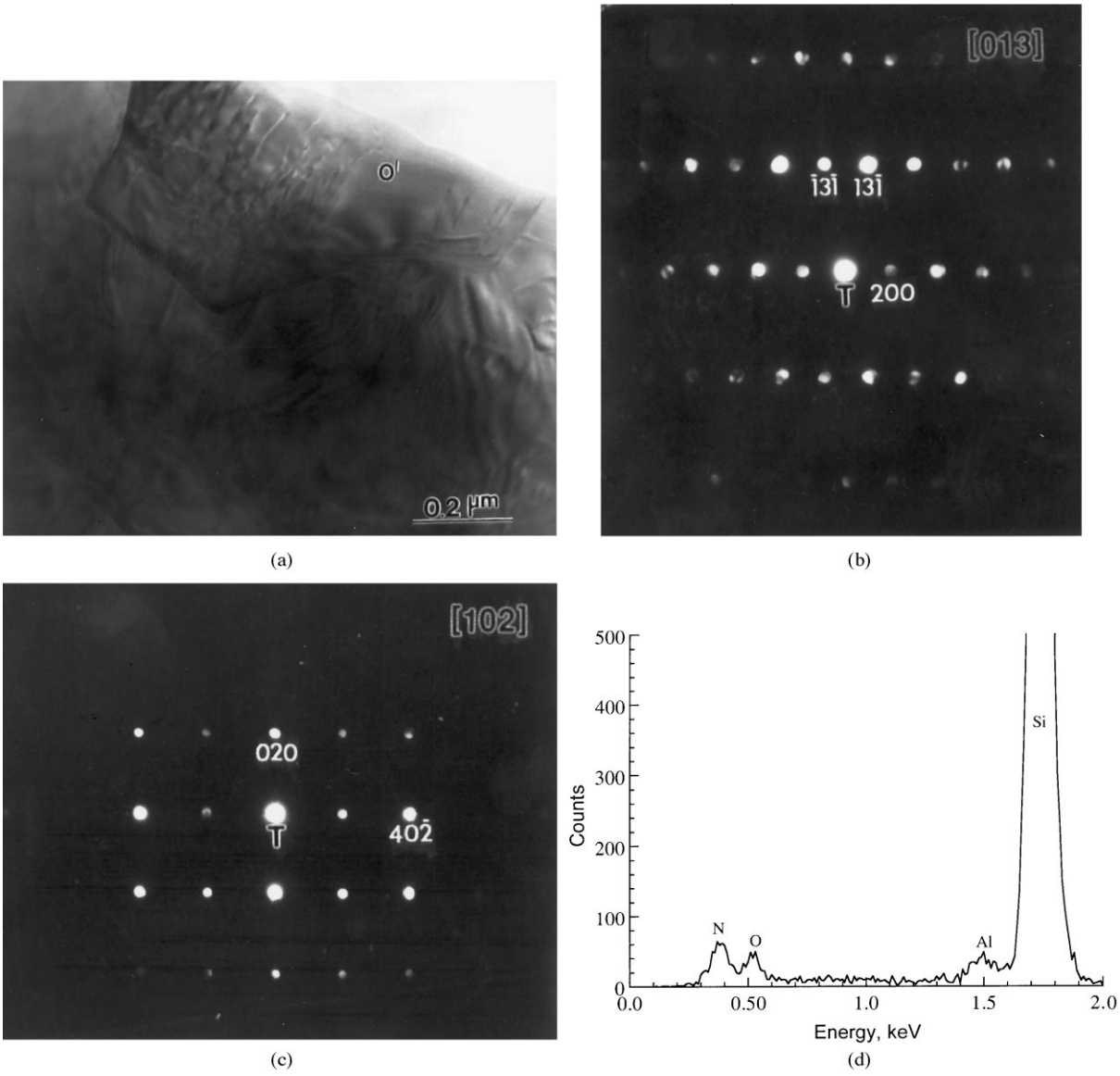

Fig. 4. (a) Bright-field TEM micrograph showing O-sialon grains containing a high density of defects. (b,c) SADPs from O-sialon. (d) EDS X-ray spectrum from O-sialon showing a high oxygen content relative to nitrogen and very little aluminum.

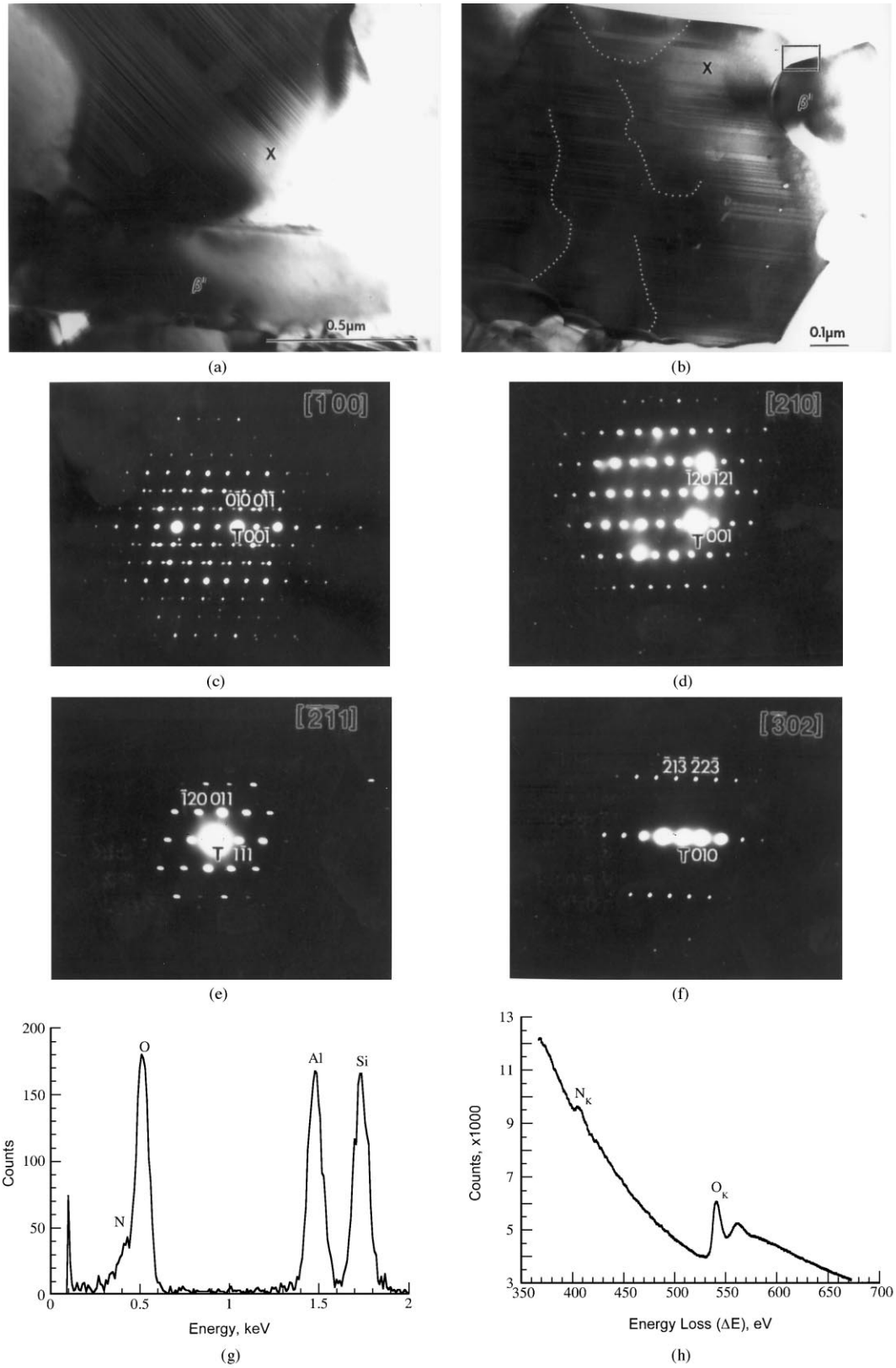

Fig. 5. (a) Bright-field TEM micrograph showing a large X-sialon grain in contact with an elongated β-sialon grain. A high density of twins of variable thickness may be noticed in X-sialon. (b) Bright-field TEM micrograph of X-sialon showing numerous twins and many antiphase domain boundaries (some of them are marked with white dots). The high-resolution image of the area marked in the box is shown in Fig. 8. (c–f) are the SADPs from X-sialon and they are indexed on the basis of a triclinic structure. Nanoprobe (g) EDS X-ray spectrum and (h) PEELS spectrum from an X-sialon grain showing relatively low nitrogen content. The PEELS spectrum also shows edges charcateristic of bonding.

Besides β-Si_3N_4, β-sialon, and O-sialon grains, sparsely distributed large irregular shaped grains of X-sialon were also observed in the sintered microstructure. The presence of a small amount of X-sialon, after hot pressing or sintering of a mixture of α-Si_3N_4 and Al_2O_3, has been reported several times in the past [19,30,31]. In this work, X-sialon was characterized by transmission electron diffraction in TEM and by PEELS and EDS X-ray microanalysis in AEM. Fig. 5(a) shows a bright-field TEM micrograph of an X-sialon grain in contact with a β-sialon grain. A substructure consisting of a high density of twins of variable thickness may be noticed. Fig. 5(b) is another grain of X-sialon, under imaging condition different from Fig. 5(a), showing a large number of twins and anti-phase domain boundaries (APB). The observation of twins and APBs in X-sialon is consistent with earlier reports [19,32]. The presence of stacking faults has also been reported in X-sialon [33,34]. Nevertheless, the combined presence of APBs and twins indicates that the microstructure may be a result of a yet unknown order–disorder phase transition. APBs may originate from the impingement of clustered nuclei and are related to the ordering in aluminum and oxygen sites [32]. The origin of the high density twins, though not known, is possibly related to the relief of transformation strain. It is very unlikely that the nucleation and growth energetics of solidification would demand the presence of such high density of twins, rather they are the products of a solid-state phase transformation. Phase equilibria study of the Si–Al–O–N system has shown that X-sialon per se is solid at 1923 K [21]. Also, twins cannot be attributed to be the effect of an applied stress as they have been observed in both sintered and hot pressed materials [32]. All X-sialon grains examined in the present study showed that the twins were always arranged in a parallel manner spanning the whole grain; and there were no intersecting twins. These suggest that the parent crystal might have been highly anisotropic and/or that the transformation strain is small enough so that a polydomain microstructure is not warranted. Twins of variable thickness might have been caused by the local constraints imposed by the APBs and/or neighboring grains. This may yield zero transformation strain within the whole grain, but may not be so within each ordered domain. Fig. 5(a) and (b) and similar micrographs reported in the literature [19,32] suggest that the morphology and distribution of X-sialon is a strong function of sintering temperature. Sintering below 1973 K produces isolated irregular shaped grains while sintering above 1973 K produces acicular grains.

Several compositions of X-sialon have been reported in the literature [20,21,29,35–43]. Recent results of Anya and Hendry [33] suggest that X-sialon exists over a narrow composition range. Like its composition, the structure of X-sialon is also controversial. The structure of X-sialon has been investigated by both electron [32,33,41] and X-ray diffraction [20,33,44,45]. Discrepancies between X-ray diffraction and electron diffraction data exist and they originate due to the presence of a high density of twins and stacking faults on a very fine scale. It has been argued that the electron diffraction pattern obtained from X-sialon can be indexed equally well on the basis of a microstructure containing a high density of microtwins or on that of a periodically faulted structure [34]. Several SADPs were obtained either by tilting the same grain or from different grains. Only four SADPs are shown in Fig. 5(c)–(f). They are indexed in terms of a triclinic structure using the lattice parameters reported by Zangvil [44]. Fig. 5(g) shows a nanoprobe EDS X-ray spectrum from X-sialon. This EDS X-ray spectrum is very distinct from those of

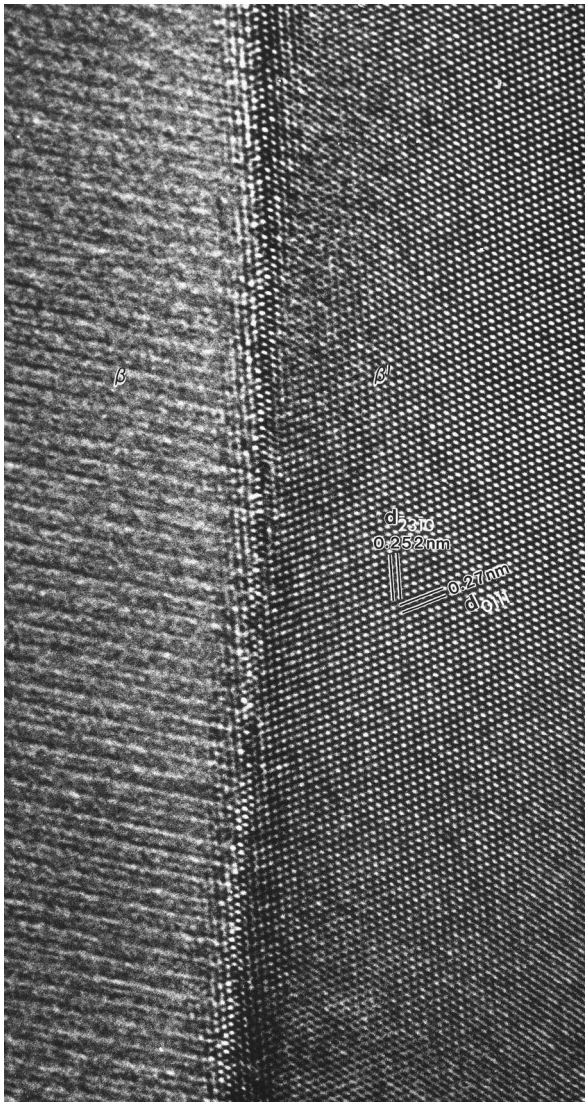

Fig. 6. HREM micrograph showing the interface between β-sialon and β-Si_3N_4 grains. The β-sialon grain is oriented along the $[\bar{4}\ \bar{1}\ 5\ 6]$ zone axis. The absence of any intergranular glassy phase may be noticed.

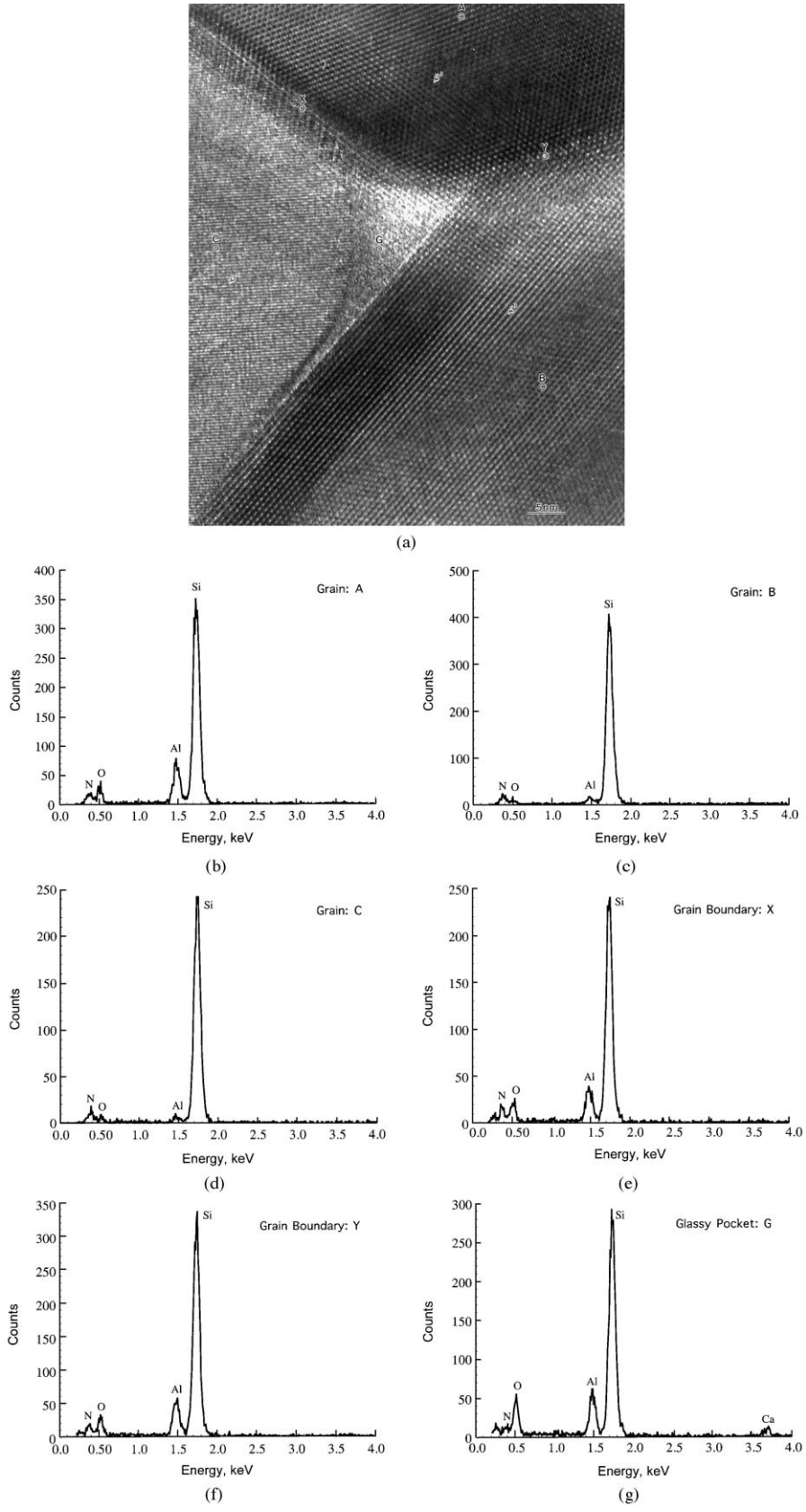

Fig. 7. (a) HREM micrograph showing a triple junction involving β-sialon that shows the presence of a glassy pocket. The circles represent the positions from where the nanoprobe EDS X-ray spectra were collected. Nanoprobe EDS X-ray spectra from: (b) the interior of grain A, (c) the interior of grain B, (d) the interior of grain C, (e) the grain boundary marked X, (f) the grain boundary marked, and (g) the glassy pocket G. The presence of calcium in (g) may be noted.

β-sialon. The presence of nitrogen, though not so obvious in Fig. 5(g), can be clearly seen in the corresponding PEELS spectrum shown in Fig. 5(h). The composition of the X-sialon was not quantified in this work. The EDS X-ray and PEELS spectra shown in Fig. 5(g) and (h), respectively, were taken from the center of an X-sialon grain.

The absence of a glassy phase at the interphase interfaces is highly desirable for improving the high-temperature properties. While there is a variety of techniques to detect the intergranular glassy phase, the present work examined 25 interphase interfaces including nine triple junctions by HREM. Fig. 6 shows an HREM image of the interface between β-sialon and β-Si_3N_4 grains. The β-sialon grain is oriented along the $[\bar{4}\ \bar{1}\ 5\ 6]$ zone axis. The measured lattice spacings $d_{(01\bar{1}1)}$ and $d_{(\bar{2}3\bar{1}0)}$ are 0.27 and 0.252 nm, respectively. These values gave $a=0.77$ nm and $c=0.295$ nm. Using the known lattice parameters [18] of β-sialon ($Si_{6-z}Al_zO_zN_{8-z}$), the β-sialon shown in Fig. 6 corresponds to a z value of ~2.5 or ~35 equivalent% of Al. The absence of any intergranular glassy film may be noticed in Fig. 6. Due to crystallographic (anisotropic) and temperature (isotropic) dependencies of surface energies, Clarke and Thomas [46] have argued that, at low temperatures, an intergranular glassy phase may not wet all boundaries, thus it may not be visible at all interfaces. Later, Kleebe et al. [11,47] also reported that low-angle and special boundaries are not covered with intergranular glassy films. In such situations, the glassy phase may be concentrated at 3- and 4-grain junctions [46]. In the present work, triple junctions involving β-sialon grains, both with and without a glassy pocket, were observed. Fig. 7(a) shows a triple junction involving β-sialon that contains a glassy pocket. Fig. 7(b)–(g) show the nanoprobe EDS X-ray spectra obtained from the interior of the grains [marked A, B, and C in Fig. 5(a)], the interphase interfaces [marked X and Y in Fig. 5(a)], and the glassy pocket [marked G in Fig. 5(a)]. The EDS X-ray spectrum obtained from the glassy pocket, shown in Fig. 7(g), contained a noticeable amount of calcium as an impurity, while those obtained from the grain interiors and interfaces did not show the presence of calcium. This is consistent with the notion that a pre-existing silicate liquid acts as sink for larger impurity ions, such as Ca^{2+}. Fig. 8 shows an HREM image of a triple junction involving X-sialon, β-sialon and β-Si_3N_4 grains. Not only is the triple junction devoid of a glassy pocket, the interphase interfaces X-sialon/β-sialon and X-sialon/β-Si_3N_4 are also devoid of glassy films. There

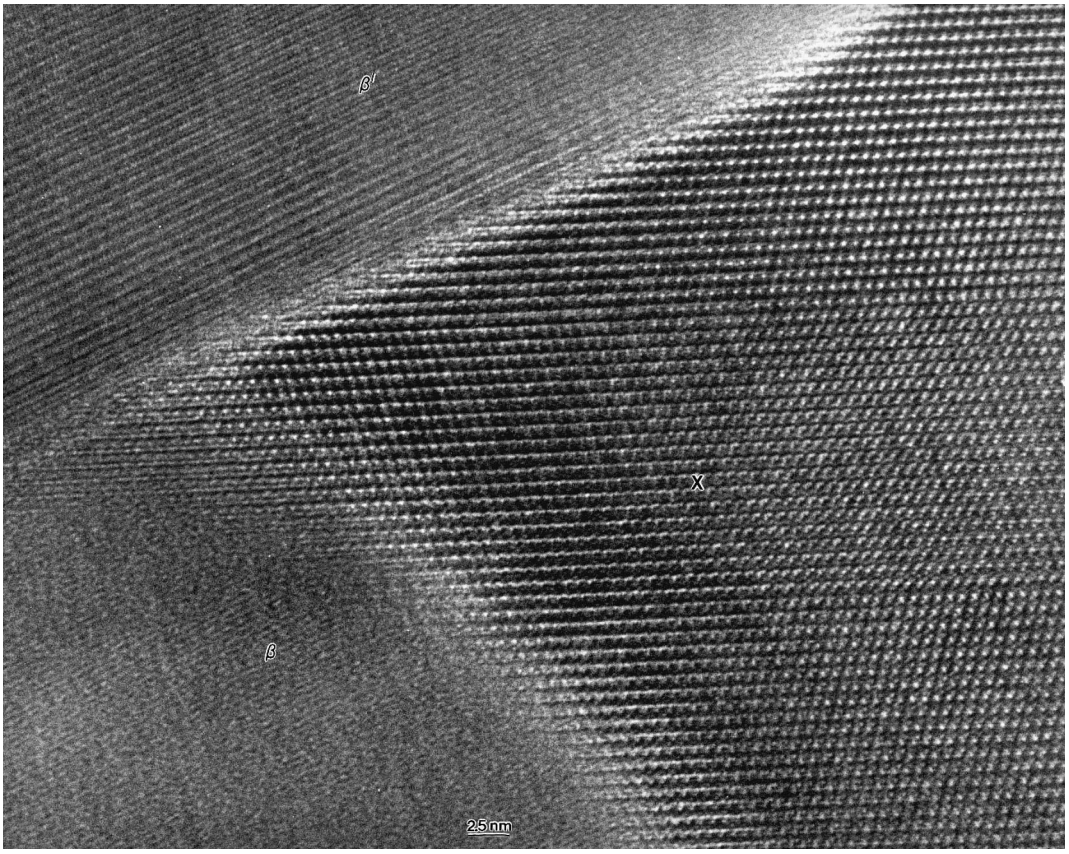

Fig. 8. HREM micrograph showing the absence of any glassy pocket at the triple junction involving X-sialon, β-sialon and β-Si_3N_4. The interphase interfaces (X-sialon/β-sialon and X-sialon/β-Si_3N_4) are also devoid of any glassy phase.

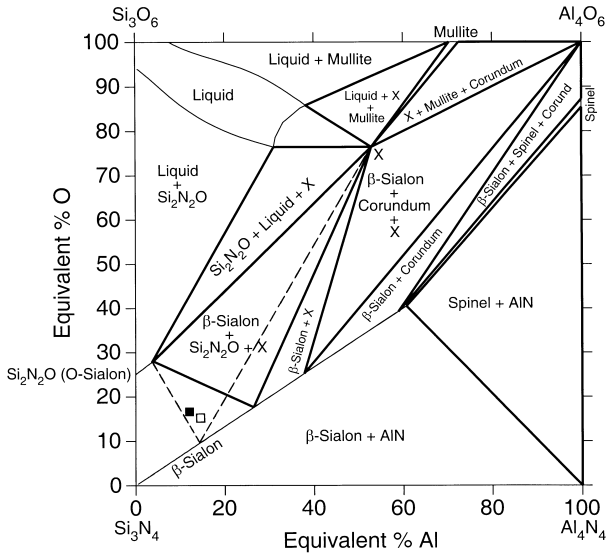

Fig. 9. Calculated isothermal section of the Si–Al–O–N system at 1923 K. The composition of the ceramic in this study is shown by a filled square. The data of Vleugels and van der Biest [19] are shown by the open square. The dashed line is the revised phase boundary.

is no published report on the interphase interfaces of sintered β-Si_3N_4 coated with alumina. Nevertheless, only occasional observations of interfaces without intergranular glassy film in β-sialon ceramics produced by conventional powder blending methods have been reported [9,18]. It is well known that, by minimizing and possibly eliminating the intergranular glassy phase, the high-temperature properties of sialon ceramics can be improved significantly. The use of a mixture of "balanced" powder composition [48] [49] and sialons containing YAG [50] may also minimize the amount of glassy phase.

The observation of three phases β-sialon, O-sialon and X-sialon in the ceramic is in slight disagreement with the calculated [51] phase diagram in the sense that the overall composition lies just outside the above three-phase field. In fact, the experimental data of phase relations involving the above three phases, as reported by Vleugels and van der Biest [19], are also in disagreement with the calculated three-phase field. The revised (β - sialon + O - sialon)/(β - sialon + O - sialon + X - sialon) phase boundary, including the present data and that after Vleugels and van der Biest [19], is shown by the dotted line in Fig. 9.

4. Conclusions

To the authors' knowledge, this is the first detailed microstructural study of sintered β-Si_3N_4 coated with an amorphous alumina. Coating of β-Si_3N_4 powder with alumina followed by hot pressing and reactive sintering offers a unique opportunity to design β-sialon ceramics desirable for high-temperature applications. The microstructure of the produced ceramic consisted of β-Si_3N_4, β-sialon, O-sialon, and X-sialon. The characteristic microstructural features of the phases present in this ceramic are as follows. Unreacted β-Si_3N_4 grains are polyhedral and nearly equiaxed. β-sialon grains (of variable composition) are both polyhedral and elongated along the *c*-axis with variable aspect ratios. Elongated grains of O-sialon contain a high density of defects. X-sialon grains are blocky in shape and very oxygen-rich. Even though the β-sialon grains were relatively small, they had high aspect ratio. HREM examination of several interphase interfaces and triple junctions suggests that the amount of glassy phase in the present ceramic is substantially lower compared to those reported in the literature. Further systematic study is needed to understand and control the sintering mechanism and microstructural evolution during sintering of β-Si_3N_4 particles coated with amorphous alumina.

Acknowledgements

This work was financially supported by the National Science Foundation under a Small Grant for Exploratory Research (Grant# 92-23584). One of us (G.G.) would like to thank Dr. Lucia Dumitreseu of Royal Institute of Technology, Stockholm, for her help in the calculation of Si–Al–O–N phase diagrams.

References

[1] W. Dressler, M.J. Hoffmann, G. Petzow, Correlation among powder characteristics, microstructural development and fracture toughness of Si_3N_4, Key Eng. Mater. 89–91 (1994) 165–170.
[2] P. Saigalik, J. Dusza, M.J. Hoffmann, Microstructural design of reinforced Si_3N_4 ceramics with respect to the toughening mechanisms, Ceramica Acta 6 (1994) 35–41.
[3] P. Saigalik, J. Dusza, M.J. Hoffmann, Relationships between microstructure, toughening mechanisms, and fracture toughness of reinforced silicon nitride ceramics, J. Am. Ceram. Soc. 78 (1995) 2619–2624.
[4] Y. Okamoto, N. Hirosaki, Y. Akimune, M. Mitorno, Mechanical properties and oxidation resistance of silicon nitride produced from low purity β-powder, J. Ceram. Soc. Japan 103 (1995) 720–723.
[5] T.-S. Sheu, Microstructure and mechanical properties of the in-situ and Si_3N_4/α′-Sialon composite, J. Am. Ceram. Soc. 77 (1994) 2345–2353.
[6] N. Hirosaki, Y. Okarnoto, Y. Akimune, T. Yamada, M. Mitorno, Sintering of β-Si_3N_4 powder made by the imide-decomposition method, J. Ceram. Soc. Japan 103 (1995) 977–978.
[7] T. Ekström, M. Nygren, Sialon ceramics, J. Am. Ceram. Soc. 75 (1992) 259–276.
[8] M.K. Cinibulk, G. Thomas, S.M. Johnson, Fabrication and secondary-phase crystallization of rare-earth disilicate–silicon nitride ceramics, J. Am. Ceram. Soc. 75 (1992) 2037–2043.
[9] Y. Goto, G. Thomas, Microstructure of silicon nitride ceramics sintered with rare-earth oxides, Acta Metall. Mater. 43 (1995) 923–930.

[10] R. Raj, F.F. Lange, Crystallization of small quantities of glass (or a liquid) segregated in grain boundaries, Acta Metall. 29 (1981) 1993–2000.
[11] H.J. Kleebe, M.J. Hoffmann, M. Rühle, Influence of secondary phase chemistry on grain boundary film thickness in silicon nitride, Z. Metallkde. 83 (1992) 610–617.
[12] M. Kulig, W. Oroschin, P. Griel, Sol–gel coating of silicon nitride with Mg–Al oxide sintering aid, J. Eur. Ceram. Soc. 10 (1989) 209–217.
[13] C.-M. Wang, F.L. Riley, Alumina-coating of silicon nitride, J. Eur. Ceram. Soc. 10 (1992) 83–93.
[14] C.-M. Wang, F.L. Riley, Morphological changes during the calcination of oxide-coated silicon nitride powder, in: F.R. Sale (Ed.), Novel Synthesis and Processing of Ceramics, British Ceramic Proceedings No. 53, Institute of Materials, London, 1994, pp. 235–248.
[15] H. Schmidt, G. Nabert, G. Ziegler, H. Goretzki, Characterization and surface chemistry of uncoated and coated silicon nitride powders, J. Eur. Ceram. Soc. 15 (1995) 667–674.
[16] I.J. Davies, B. Djuricic, S. Pickering, J.Th.M. De Hosson, HRTEM investigation of silicon nitride powder coated with yittrium oxide-precursor, J. Surf. Anal. 3 (1997) 394–400.
[17] H. Nakamura, A. Kato, Effect of crystallization of alumina hydrate in preparation of alumina-coated composite particles, Ceramics International 18 (1992) 201–206.
[18] T. Ekström, P.O. Käll, M. Nygren, P.O. Olsson, Dense single-phase O-sialon ceramics by glass-encapsulated hot isostatic pressing, J. Mater. Sci. 24 (1989) 1853–1861.
[19] J. Vleugels, O. van der Biest, Development, chracterization and oxidation behavior of Si_3N_4–Al_2O_3 ceramics, J. Eur. Ceram. Soc. 13 (1994) 529–544.
[20] D.P. Thompson, P. Korgul, Sialon X-phase, in: F.L. Riley (Ed.), Progress in Nitrogen Ceramics, Martinus Nijhoff, The Hague, The Netherlands, 1983, pp. 375–380.
[21] I.K. Naik, L.J. Gauckler, T.Y. Tien, The solid–liquid equilibria in the system Si_3N_4–AlN–SiO_2–Al_2O_3, J. Am. Ceram. Soc. 61 (1978) 332–335.
[22] S.-L. Hwang, I.-W. Chen, Nucleation and growth of β-Sialon, J. Am. Ceram. Soc. 77 (1994) 1719–1728.
[23] F.F. Lange, Fracture toughness of Si_3N_4 as a function of the initial α-phase content, J. Am. Ceram. Soc. 62 (1979) 428–430.
[24] H. Emoto, M. Mitomo, Control and characterization of abnormally grown grains in silicon nitride ceramics, J. Eur. Ceram. Soc. 17 (1997) 797–804.
[25] G.R. Terwilliger, F.F. Lange, Hot-pressing behavior of Si_3N_4, J. Am. Ceram. Soc. 52 (1974) 25–29.
[26] D.-D. Lee, S.-J.L. Kang, G. Petzow, D.N. Yoon, Effect of α to β phase transition on the sintering of silicon nitride ceramics, J. Am. Ceram. Soc. 73 (1990) 767–769.
[27] M. Mitomo, M. Tsutsumi, H. Tanaka, S. Uenosono, F. Saito, Grain growth during gas-pressure sintering of O-silicon nitride, J. Am. Ceram. Soc. 73 (1990) 2441–2445.
[28] M.H. Lewis, C.J. Reed, N.D. Butler, Pressureless-sintered ceramics based on the compound Si_2N_2O, Mater. Sci. Eng. 71 (1985) 87–94.
[29] T. Ekström, P.O. Olsson, O. Holmström, Sialon ceramics prepared by hot isostatic pressing, J. Eur. Ceram. Soc. 12 (1993) 165–176.
[30] K.H. Jack, W.J. Wilson, Ceramics based on the Si–Al–O–N and related systems, Nature (London) Phys. Sci. 238 (1972) 28–29.
[31] Y. Oyarna, O. Kamigaito, Hot-pressing of Si_3N_4–Al_2O_3, Yogyo-Kyokai-Shi 80 (1972) 327–336.
[32] P. Drew, M.H. Lewis, The microstructures of silicon nitride/alumina ceramics, J. Mater. Sci. 9 (1974) 1833–1838.
[33] C.C. Anya, A. Hendry, Stoichiometry and crystal structure of X-phase sialon, J. Eur. Ceram. Soc. 10 (1992) 65–74.
[34] D.R. Clarke, High-resolution techniques and application to non-oxide ceramics, J. Am. Ceram. Soc. 62 (1979) 236–246.
[35] K.H. Jack, The production of high temperature, high strength nitrogen ceramics, in: Ceramics for High Performance Applications, Brook Hill Publishing, Chestnut Hill, MA, 1974, pp. 265–286.
[36] E. Gugel, I. Petzenhauser, A. Fickel, X-ray investigation of the system silicon-nitride–alumina (on the question of a 'second' phase in the system aluminium–silicon–oxygen–nitrogen), Powder Met. Int. 7 (1975) 66–67.
[37] L.J. Gauckler, H.L. Lukas, G. Petzow, Contribution to the phase diagram Si_3N_4–AlN–Al_2O_3–SiO_2, J. Am. Ceram. Soc. 58 (1975) 346–347.
[38] R.R. Wills, R.W. Stewart, J.M. Wimmer, Effect of composition and X-phase on the intrinsic properties of reaction-sintered sialon, Am. Ceram. Soc. Bull. 56 (1977) 194–203.
[39] P.L. Land, J.M. Wimmer, R.W. Burns, N.S. Choudhury, Compounds and properties of the system Si–Al–O–N, J. Am. Ceram. Soc. 61 (1978) 56–60.
[40] M. Hoch, K.M. Nair, Preparation and characterization of ultrafine powders of refractory nitrides: II. Sialon, Am. Ceram. Soc. Bull. 58 (1979) 191–193.
[41] A. Zangvil, The structure of the X-phase in the Si–Al–O–N alloys, J. Mater. Sci. Lett. 13 (1978) 1370–1374.
[42] M. Mitomo, Y. Hasegawa, Y. Bando, A. Watanabe, H. Suzuki, The strength of hotpressed O-sialon, Yogyo-Kyokai-Shi 88 (1980) 298–304.
[43] B. Bergman, T. Ekström, A. Mieski, The Si–Al–O–N system at temperatures of 1700–1775°C, J. Eur. Ceram. Soc. 8 (1991) 141–151.
[44] A. Zangvil, L.J. Gauckler, M. Rijhle, Indexed X-ray diffraction data for the sialon X-phase, J. Mater. Sci. Lett. 15 (1980) 788–790.
[45] K.H. Jack, Sialons and related nitrogen ceramics, J. Mater. Sci. 11 (1976) 1135–1158.
[46] D.R. Clarke, G. Thomas, Grain boundary phases in a hot-pressed MgO fluxed silicon nitride, J. Am. Ceram. Soc. 60 (1977) 491–495.
[47] H.-J. Kleebe, M.K. Cinibulk, R.M. Cannon, M. Rühle, Statistical analysis of film thickness in silicon nitride ceramics, J. Am. Ceram. Soc. 76 (1993) 1969–1977.
[48] M.H. Lewis, B.D. Powell, R. Drew, R.L. Lumby, B. North, A.L. Taylor, The formation of single phase Si–Al–O–N ceramics, J. Mater. Sci. 12 (1977) 61–74.
[49] M. Mitomo, Y. Hasegawa, Y. Bando, A. Watanabe, H. Suzuki, The strength of hot-pressed β-sialon, Yogyo-Kyokai-Shi 88 (1980) 298–304.
[50] M.H. Lewis, Crystallization of grain boundary phases in silicon nitride and sialon ceramics, Key Eng. Mater. 89–91 (1994) 333–338.
[51] L. Dumitrescu, B. Sundman, A thermodynamic reassessment of the Si–Al–O–N system, J. Eur. Ceram. Soc. 15 (1995) 239–247.